Preprint of article accepted for publication in the Journal of Loss Prevention in the Process Industries, September 16, 2026. See journal for final version: https:/ /doi.org/10.1016/j.jlp.2026.106185

Autoignition Testing: Injection, Mixing, and Ignition

Charline Fouchier*, Hannah Ramsperger, Joseph E. Shepherd

Graduate Aerospace Laboratories California Institute of Technology Pasadena CA USA

Abstract

This study reports on fuel injection, vaporization, mixing, and ignition under conditions simulating standardized autoignition tests with uniform gas and surface temperatures in a closed volume. An optically accessible, instrumented, one-liter cubic test cell was fabricated from passivated metal with fused-silica windows. The cell was electrically heated from the top and bottom with feedback control to create a uniform temperature air atmosphere. Liquid fuel (n-hexane) was injected by a syringe pump to control the injected volume and rate. Vaporization and mixing of the fuel were characterized by direct imaging, infrared absorption, and background-oriented schlieren (BOS). Combustion events were captured using BOS, fine thermocouples, and direct imaging.

Results show that in a nearly uniform temperature atmosphere, fuel dispersion after vaporization is dominated by diffusion, but localized fuel concentrations can be created by convection from small temperature variations. Dispersion and ignition can occur on similar timescales, leading to ignition in a partially mixed environment. Measurements show two-stage ignition behavior in stratified atmospheres: slowly propagating cool-flame combustion followed by the formation of a rapidly propagating hot flame. High-speed imaging highlights the early formation and growth of the ignition kernel and transition between combustion modes. Two distinct ignition modes were observed, which exhibit similar temperature profiles measured by our thermocouple but differ in light emission and peak pressure. These observations suggest further refinements of autoignition test methodology.

Keywords: Thermal Ignition, Flammability, Standardized Tests, Safety, Autoignition, Vaporization, Dispersion

1. Introduction

The autoignition temperature (AIT), defined as the lowest temperature at which a fuel-air mixture ignites spontaneously without an external ignition source, is widely used as a screening parameter for safe storage, transportation, and process operation. Regulatory frameworks and engineering design guidelines often rely on AIT values to define operating limits, classify materials, and prevent accidental ignition. Despite its widespread use, AIT is not a fundamental thermochemical property of a fuel. Instead, it depends on the surrounding environment, including temperature gradients, heat losses, mixture composition, flow fields, and the characteristic timescales of mixing and chemical reaction.

Standardized test methods attempt to control these variables. The ASTM standard ASTM-E659 (2014), for instance, determines the AIT by injecting a small quantity of liquid fuel into a 0.5-liter heated vessel and visually identifying the appearance of a flame. Although widely adopted for its simplicity, this approach presents several well-documented limitations related to experimental control and representativeness. The measured AIT is known to be sensitive to factors related to the apparatus, such as vessel size, geometry, and material, as well as the heating rate and thermal uniformity (Setchkin, 1954; NFPA, 1991). Flask aging, surface contamination, and ambient temperature have also been shown to systematically bias

*Corresponding author

Email address: charline@caltech.edu (Charline Fouchier)

AIT measurements (Chen and Hsieh, 2010; Martin, 2023). These parameters are not explicitly controlled by the standard and can cause significant discrepancies between laboratories despite adherence to the same protocol.

Ignition behavior depends not only on intrinsic fuel reactivity but also on details of the injection process, fuel vaporization, and dispersion within the vessel. Even subtle variations in convection patterns or dispersion rates can influence the apparent ignition temperature, leading to ambiguity and inter-laboratory variability. Understanding the physical processes that occur inside the vessel, particularly fuel evaporation, transport, mixing, and the subsequent ignition sequence, is therefore essential for interpreting AIT measurements and improving the reliability of standard test procedures.

Recent work has begun to address these challenges. Martin and Shepherd (2021) conducted experiments that identified multiple ignition modes distinguished by flame luminosity and temperature evolution. In particular, they described "Mode I" events, characterized by a bright flame and a rapid temperature rise, and "Mode III" events, which exhibited weak blue or nearly invisible flames yet showed similar temperature signatures. In the effort to characterize the autoignition behavior of aviation fuels, both modes appeared distinctly and raised important safety questions, specifically, which mode should determine the autoignition temperature limit (Fouchier and Shepherd, 2025). These findings highlighted the complexity of interpreting ignition events based solely on a single thermocouple or visual observation and emphasized the need for more detailed, multi-modal diagnostics.

Complementary numerical studies by Davis et al. investigated hexane dispersion (Davis et al., 2025) and ignition (Davis et al., 2026) inside the flask of the ASTM-E659 apparatus, resolving three-dimensional motion, molecular transport, and chemical reactions. These studies highlight the importance of transient fuel-air mixing, wall-temperature distribution, and the coupled roles of diffusion and natural convection in shaping ignition behavior. A two-stage ignition process was identified, consisting of an initial cool flame followed by hot-flame propagation.

Building on these earlier efforts, the present study seeks to clarify the thermophysical and chemical processes governing autoignition in an ASTM-like environment. Fuel injection, evaporation, and dispersion were studied under controlled conditions in a cubic test cell with uniform thermal conditions. High-speed imaging, infrared absorption, background-oriented schlieren (BOS), and fine-wire thermocouples are employed to characterize the evolution of vapor concentration fields and ignition kernels. This work provides new insight into the mechanisms underlying AIT measurements and offers guidance for refining standard test protocols.

2. Material and Methods

2.1. Experimental cell and instrumentation

The experiments were conducted in a one-liter cubic cell (10 cm × 10 cm × 10 cm) fabricated from metal (stainless steel and aluminum) and 2 mm-thick quartz windows to provide optical access on four sides. A plan view is shown in Fig. 1 and photos of the setup are shown in Fig. 2. All internal metallic surfaces were passivated to minimize chemical interactions with the fuel. Two pressure-relief vents, designed to open automatically in the event of an overpressure, were installed on the top plate of the cell.

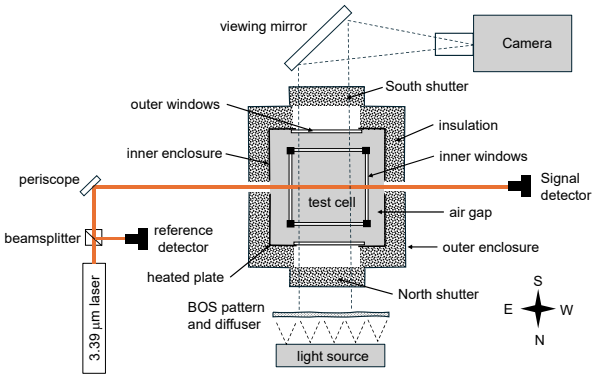
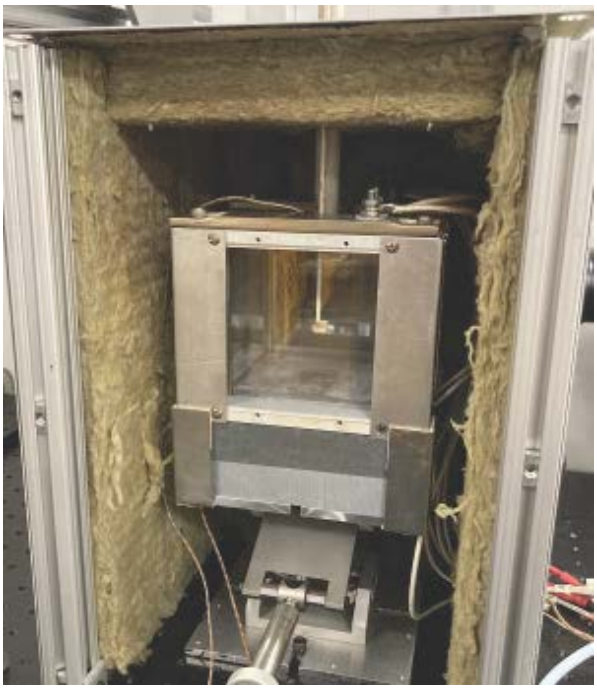


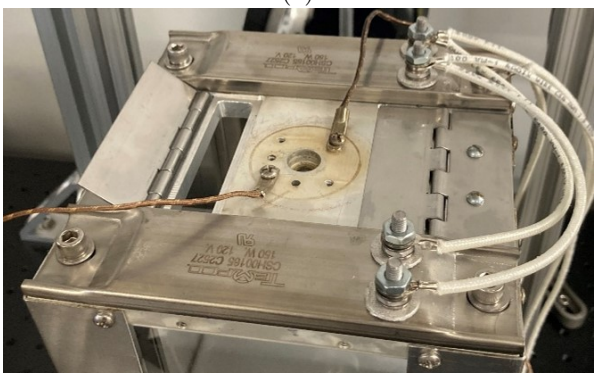
Figure 1: Plan view of test cell and diagnostics as arranged for BOS tests. Shutters are raised prior to a test. The BOS pattern and light source are replaced by the sCMOS camera, spectrometer and photodiode for the emission testing shown in Fig. 3

To ensure stable thermal conditions, the chamber was enclosed within an aluminum housing lined with glass wool insulation. Only the bottom of the cell was left uncovered by glass wool. When testing was not in progress, the windows used for visualization were covered with thermally insulated shutters. The top and bottom plates of the cell were heated by feedback-controlled electric heaters, enabling precise temperature control on the upper

and lower surfaces of the chamber. The top and bottom plates were connected by aluminum sheets on all four sides to help maintain a uniform temperature. Secondary windows were installed on the two visualization sides to control natural convection. Temperature was measured at the top and bottom plates of the cell, as well as in the middle, with 34-gauge type K thermocouples from Omega, connected to an NI-9213 C Series Temperature Input Module and a cDAQ-9171 CompactDAQ chassis from National Instruments.



(a)



(b)

Figure 2: (a) North side view of experimental test cell and surrounding insulation. (b) Top view showing heaters and vents, one open and one closed.

Fuel was introduced from the top of the chamber using a 30.5 cm long (12 inches), 26-gauge (inner diameter of 260 μm) stainless-steel needle, connected to a computer-controlled syringe pump (Model 1000-US/SyringeONE). The needle was mounted on a manually operated, sliding fixture to enable repeatable control of the injection location. This configuration allowed for accurate control of the injection parameters (volume, velocity, and height), ensuring reproducible initial conditions for each experiment.

The experiments were conducted using a combination of optical diagnostics to characterize both the fuel vapor and the combustion processes. The West-East sides of the cell were used for infrared (IR) laser absorption measurements to quantify vapor dispersion along a horizontal line at mid-height, providing data on the evolving fuel concentration. The laser path was horizontal and equidistant from the North and South windows, parallel to the path. The setup used a 2 mW, 3.39 μm He-Ne laser (Thorlabs H339P2). The 1 mm output-diameter beam passed through an electronic shutter (used for pre-test baseline correction) and a 50/50 beam splitter. Two amplified InAsSb photodetectors (Thorlabs PDA07P2) were used to measure the laser intensity before (reference) and after (measurement) the cell. Bandpass filters (3330 nm center, 150 nm width, Thorlabs 3330-150) were used in front of the detectors to minimize contamination of the signal by thermal emission from the cell. The signals were low-pass filtered at 1 kHz and recorded using a PicoScope 4424 at 2 kHz. The measurement detector $I(t)$ and reference detector I_0 signals were analyzed using the Beer-Lambert absorption law

$$I(t) = I_0 \exp(-\sigma \bar{c}(t) \ell) \,, \quad \bar{c}(t) = \frac{1}{\ell} \int_0^\ell c(x,t)\, \mathrm{d}x \,. \tag{1}$$

to measure the fuel concentration $\bar{c}(t)$ averaged over the path length ℓ =10 cm at selected vertical locations within the cell. The absorption cross section for hexane $\sigma = 40$ m^2·mol^{-1} was previously measured by Mével et al. (2012). The concentration data were filtered at 10 Hz to reduce noise that occurs at high concentrations.

The North-South sides of the cell were either used for background-oriented schlieren (BOS) or light-emission visualization. BOS imaging was used to visualize the density gradients generated by the fuel vapor and flames during injection, dispersion, and ignition. BOS provides a path-integrated mea-

surement. The refractive-index variations occurring throughout the three-dimensional volume of the cell are optically integrated and projected onto a two-dimensional image. As a result, the BOS images represent the cumulative effect of light deflection due to all density gradients along the camera's viewing direction. The setup consisted of a Phantom v2512 high-speed camera equipped with a 105 mm Nikon macro lens on one side of the cell, and a diffusive, patterned background on the opposite side, made from white paper with a printed random dot pattern, ground float glass, and a white LED (Light Emitting Diode) array for illumination. Images were acquired at 600 Hz, with an exposure time of 650 µs. PIVlab (Stamhuis and Thielicke, 2014), an open-source MATLAB software for Particle Image Velocimetry, was used to process the data by correlating each experimental image with the first image captured just before the needle was inserted for fuel injection. Interrogation windows of 64 × 64 pixels, refined to 8 × 8 pixels over three steps with 50% overlap, were used. High displacement values of the dot pattern highlighted regions with steep index of refraction gradients caused by high fuel vapor concentration or gradients in temperature associated with thermal convection or flame propagation.

The light emission inside the cell was investigated using three complementary diagnostics. Chemiluminescence from OH radicals produced during combustion was recorded with an intensified scientific sCMOS (scientific Complementary Metal-Oxide-Semiconductor) camera (PCO.DICAM C1) equipped with a 313 nm bandpass filter (10 nm FWHM) and a 50 mm objective lens. The sCMOS camera acquired images at 50 to 100 Hz with a 100 µs exposure time and a 1100 V intensifier voltage, using 2×2 binning to enhance the signal. In parallel, broadband light emission (400-1100 nm) was monitored with an amplified Si-photodetector (Thorlabs PDA100A) fitted with a 16 mm Navitar objective. A beam-splitter, optical relay lenses, and CMOS camera (Zelux CS165MU) were used to simultaneously view the detector field of view to align the photodetector. The signal from the photodetector was recorded by the PicoScope simultaneously with the two IR photodetectors. Images of the broadband luminosity were also recorded with the Phantom v2512. The arrangement of instruments for light emission measurements is shown in Fig. 3.

The syringe pump (NE1000) and the thermocouple acquisition were controlled with LabVIEW software. All instruments, except the thermocouple, were triggered by a TTL (Transistor-Transistor Logic) signal generated by the syringe pump at the start of injection. The TTL signal from the syringe pump was attenuated from 5 V to 500 µV and acquired by the thermocouple cDAQ module to synchronize the temperature measurement with the rest of the instrumentation.

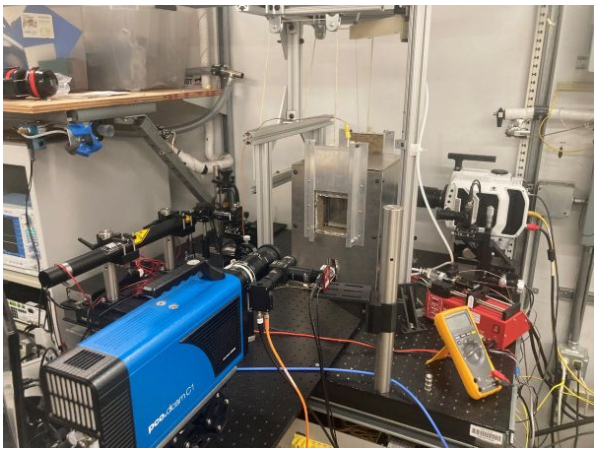


Figure 3: Experimental setup showing light emission diagnostics with the insulating shutters raised in preparation for a test.

2.2. Experimental methods

Most of the tests were conducted under conditions that closely matched the ASTM requirements for uniform gas and surface temperature within the cell. To do this, the top and bottom plates were controlled to a common temperature as closely as possible, within ±0.2°C. The insulation surrounding the cell, the aluminum construction, and secondary windows help maintain a uniform temperature within the cell. For each test, the cell temperature was monitored with the thermocouple at the center (T0). A test begins once the temperature has stabilized, which is defined as T0 varying by no more than 0.2 °C/min. Some heat loss and resulting temperature nonuniformity are inevitable due to losses through the exposed windows when the thermal shutters are open, so the fuel injection commenced as soon as the shutters were raised.

The reference signals of the laser photodetectors (background without laser and background with laser without absorption) are first recorded for 10

seconds. These results are used as part of the processing procedure to correct for baseline offsets and the absorption due to the optical components. The temperatures at the bottom, middle, and top of the cell are measured for 5 seconds immediately before initiating each experiment. The mean values are used as initial conditions. The thermal shutters are then raised to provide optical access for the North-South windows, and the injection needle is positioned inside the cell, with its tip located at mid-height. Fuel injection is carried out, which triggers the acquisition of all diagnostic instruments. After the end of the injection, the needle is removed from the cell, and data acquisition continues until either combustion is complete or the acquisition times out.

At the conclusion of each experiment, the cell atmosphere is purged of combustion products or residual fuel vapor using a metal tube inserted into the chamber, delivering compressed air for 30 seconds. The signal from the photodetector used for concentration measurements is monitored to verify that it has returned to its pre-test value, confirming that all combustion products have been removed from the cell. The thermal shutters are closed, and if necessary, a new temperature set point is established for the heater controllers. The operator then waits for the T0 temperature to re-stabilize before conducting the next experiment.

The repeatability of the tests has been verified by conducting multiple measurements under conditions maintained as closely identical as possible, with the fuel concentration evolution over time varying by less than 8% between tests. An example of the repeatability tests is shown in Figure 4, where 100 μL of hexane was injected into the cell while the cell temperature was maintained at 98.9±1°C. The laser absorption measurement was taken at the center of the cell, 5 cm above the bottom, and converted to the molar concentration of hexane using Eq.(1).

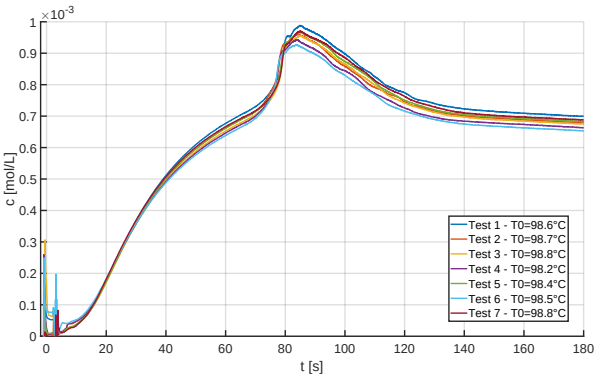


Figure 4: Test repeatability using path-averaged concentration $\overline{c}(t)$ measurements for seven tests with the laser path in the middle of the cell. Injection of 100 μL of hexane with a cell temperature of ∼99°C.

3. Results and discussion

Experimental test campaigns were conducted to separately examine the issues associated with fuel injection, dispersion, and ignition. Selected results for each campaign are described with a discussion of key points.

3.1. Injection and initial vaporization

The injection process consists of injecting between 50-200 µL of fuel through the needle. The fuel was contained in a 25 mL gas-tight syringe and injected at a rate of 5 mL/min (83 µL/s) through tubing connected to the needle. Fuel is flushed through the tubing and needle prior to each test to ensure delivery of the correct fuel amount. Immediately prior to fuel injection, the needle was inserted downward into the test cell through a narrow channel in a ceramic insulator in the center of the top of the cell.

The fuel emerges as a stream of droplets from the needle tip located at about 5 cm above the lower surface of the cell. For the fuel jet parameters in the present tests, the Weber number $\rho U^2/\sigma$ is sufficiently larger than unity (≥ 20) that the jet breaks up into droplets of about 0.5 to 1 mm diameter by the Rayleigh mechanism (Kirar et al., 2024). The droplets splash and migrate across the bottom surface of the test cell, evaporating due to heat transfer from the hot surface and the surrounding hot atmosphere. The fuel vaporizes, warms up, and spreads across the bottom of the test cell to form a stably stratified layer that begins slowly diffusing upward. This creates a layer of dense fuel vapor at the bottom of the cell within a few seconds after the cessation of injection. The fuel vapor is dense due to the higher molar mass (86 g/mol) and lower temperature as the injected fuel is at room temperature and cools the surrounding atmosphere during vaporization.

The impact (Liang and Mudawar, 2017) and vaporization (Mizomoto et al., 1978; Mizomoto and Ikai, 1978; Mizomoto et al., 1979) of an alkane fuel droplet on a hot surface depend on a number of fac-

tors such as the material and finish of the surface, the interfacial tensions between liquid, surface, and gas, the size and impact velocity of the droplets, and the surface temperature. For cold drops impacting hot surfaces, the most important parameter is the surface temperature relative to the temperatures characterizing the boiling behavior. For the present tests, these characteristic fuel temperatures include the boiling point T_B, the Nukiyama temperature T_N (surface temperature corresponding to the shortest evaporation time), and the Leidenfrost temperature T_L (surface temperature at which a vapor layer forms between the surface and the liquid, substantially increasing the evaporation time). Discussion of the Nukiyama and Leidenfrost temperatures and their effect on droplet vaporization rate can be found in Mills and Fry (1982a). For surface temperatures below T_L, the droplet remains in full contact with the surface, where nucleation and boiling occur within the liquid, resulting in high heat transfer and vaporization rates. For surface temperatures above T_L, the droplet is suspended on a cushion of vapor that reduces the heat transfer rate and vaporization rate. Figure 5 illustrates the change in hexane droplet contact and vaporization for several temperatures, with a field of view of approximately 27 mm x 15 mm centered on the middle of the bottom plate. The figure shows droplets' behavior during vaporization (T0 = 50.6°C), boiling (T0 = 69.0°C), transition between boiling and Leidenfrost vaporization (T0 = 99.0°C), and Leidenfrost vaporization (T0 = 160.4°C). The temperature measured by T0 (i.e., the temperature at the center of the cell) is reported, as it is used as the reference temperature for all tests. Significant effort was made to ensure a uniform temperature distribution within the cell; consequently, the surface temperature differs from T0 by no more than 2°C.

For the n-hexane fuel used in the present tests, T_B = 69°C, T_N = 110-120°C, T_L = 130-135°C as measured by Mills and Fry (1982b). The lifetime of a droplet decreases with increasing surface temperature until T_N is reached and then abruptly increases (by up to a factor of 5) when T_L is exceeded (Mizomoto et al., 1978). Both T_N and T_L are linearly proportional to T_B (Mills and Fry, 1982b) for alkane fuels. Boiling point increases with fuel molar mass or equivalently carbon number for alkanes, but the AIT is only weakly dependent on carbon number, slightly decreasing with increasing carbon number from 225°C for n-hexane (C6) to 200°C for n-tetradecane (C14). As a consequence, n-hexane droplets impacting a surface at or above the AIT temperature are suspended on a vapor layer due to the Leidenfrost effect, while droplets impacting surfaces at or below 100°C vaporize due to full contact boiling within the drop.

The situation with aviation fuels like Jet-A is more complex due to the multi-component composition. Werner et al. (2024) found that for one aviation kerosene (F-24 specification), the transition from full contact to Leidenfrost for single droplets occurred at 277°C, while for one synthetic fuel (ATJ process), the transition occurred at 327°C. Our previous investigation (Fouchier and Shepherd, 2025) found that for two Jet A-like fuels, the AIT (50% ignition probability) was between 228-233°C and for one synthetic fuel, 202-214°C, indicating that vaporization will occur in the full contact mode during AIT testing for these fuels.

Figure 6 shows a sequence of BOS images taken after the injection of 100 µL of hexane into a hot-air atmosphere at temperatures lower and above the Leidenfrost temperature of the fuel. The field of view measures approximately 100 × 50 mm, and the injection needle is visible just below the top of the frame. The colors are proportional to the background displacement (red high, blue low), which is a measure of the line-of-sight averaged gradients in the refractive index (Raffel, 2015) created by density and fuel concentration gradients. The first frames show the droplet stream impinging on the bottom of the test cell, droplets migrating across the surface, and vaporizing. The next set of frames shows the lateral dispersion of the fuel layer and the start of upward diffusion. The vaporization behavior is directly influenced by surface temperature. When the surface temperature exceeds the Leidenfrost temperature, the vaporization rate decreases, leading to slower and more localized vaporization.

3.2. Dispersion and Mixing

The dispersion and mixing of the fuel in a hot atmosphere were investigated at three different heights inside the cell, at different injected volumes, and at different cell temperatures.

The dispersion of the fuel in a hot atmosphere was evaluated by measuring the hexane concentration at three different heights inside the cell, with each height assessed in a separate test. The heights, referenced from the bottom of the cell, were set at one-quarter, one-half, and three-quarters of the total cell height. The three signals in Fig. 8a illustrate

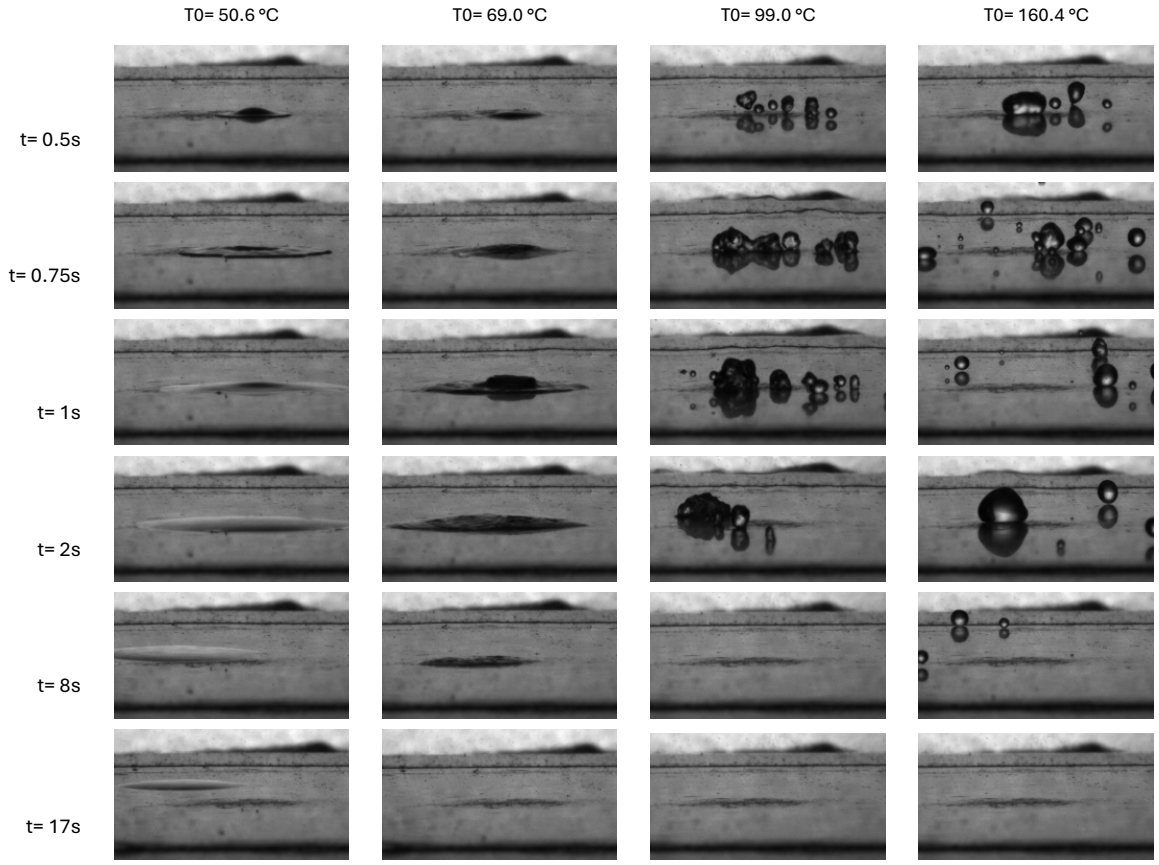


Figure 5: Sequence of direct images of hexane droplet vaporization at several temperatures for selected times. The camera is focused on the region of droplet impact and oriented to view the cell lower surface. T0 is the temperature in the middle of the cell.

several features of the dispersion process for 100 μL of hexane and a cell temperature of ∼99°C.

Immediately after injection and vaporization, the fuel forms a dense layer at the bottom of the cell due to the higher molar mass of hexane and a decrease in the gas temperature due to vaporization. The hexane diffuses upward and mixes with the air, resulting in the peak concentration decreasing with time and with increasing height in the cell. The initially high concentration at the bottom results in a broad maximum at around 25 s for the $H/4$ location. The location of the maximum shifts later in time for the $H/2$ location, and the concentration measured at $3H/4$ does not show a pronounced peak and rises smoothly to a maximum value at 110 s and then slowly decays. After 140 s, the fuel concentrations at all three locations approach a common value, indicating the fuel is well mixed with the air in the cell after this time.

Injection and vaporization of the liquid fuel result in a layer of heavy gaseous fuel at the bottom of the cell. The atmosphere is initially observed to be quiescent due to the uniform initial temperature, and the fuel layer is stably stratified. The fuel immediately begins dispersing into the air above through the combined processes of diffusion and convection to create a fuel-air mixture. Diffusion alone will result in smooth and slow variation of the fuel concentration within the cell. An order-of-magnitude estimate of the diffusion time is H^2/D, where D is the binary diffusion coefficient and H is the cell height (10 cm). The binary diffusion coefficient was evaluated from gas kinetic theory using Cantera (Goodwin et al., 2023). As shown in Fig. 7, D increases with increasing temperature: $D = 8.69\times 10^{-6}$ m^2·s^{-1} at 50°C; 1.14×10^{-5} m^2·s^{-1} at 100°C;

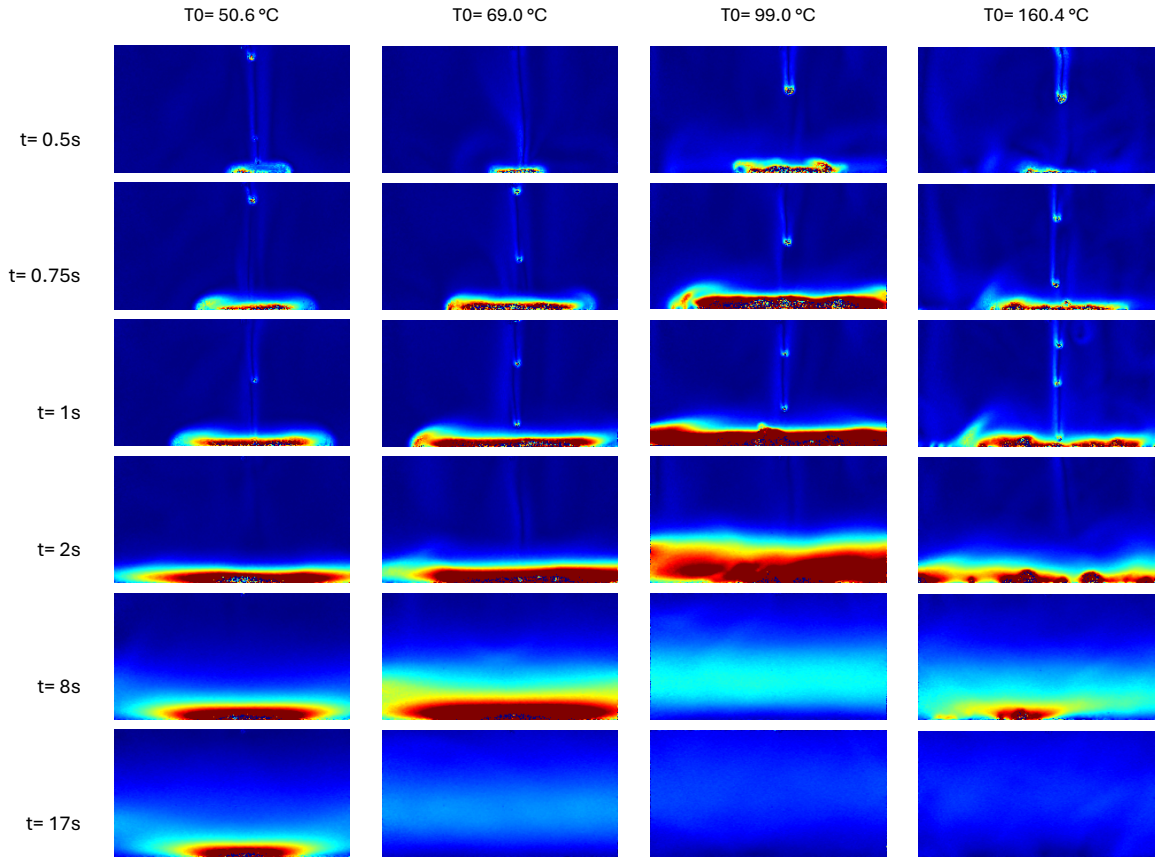


Figure 6: Sequence of BOS images showing liquid hexane droplet injection and vaporization at several temperatures for selected times following injection. T0 is the temperature in the middle of the cell.

$1.78\times\ 10^{-5}$ $m^2{\cdot}s^{-1}$ at 200°C.

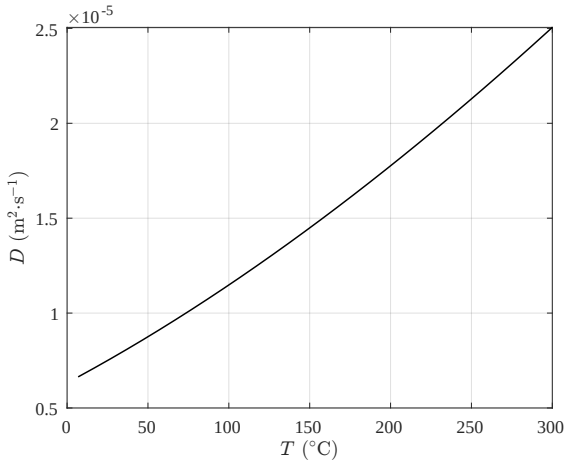


Figure 7: Binary diffusion coefficient for mixtures of n-hexane and N_2 as a function of temperature.

The diffusion characteristic time is on the order of 6-11 s for the conditions of our tests. However, the results of numerical simulations and our experiments indicate that the actual time required to well mix the fuel by diffusion is on the order of 50-200 s, 10-20 times longer than the naive order-of-magnitude estimate. The fuel concentration is highly nonuniform before the mixing time has elapsed. As a consequence, autoignition likely takes place within a nonuniform mixture, similar to predictions (Davis et al., 2025, 2026) for ASTM testing with modest ignition times.

Fuel injection and vaporization cause gas motion and stirring near the lower surface of the cell. However, the BOS visualization (Fig. 6) indicates that this motion dies out quickly, within 10 s, resulting in a stably stratified mixture of fuel and air with concentration and density mainly varying with height. As a consequence, fuel dispersion for

these cases is dominated by vertical diffusion once the initial perturbation dies down. However, small temperature differences within the cell that result in heat losses through the windows, mainly when the thermal shutters are opened at the start of a test, can induce natural convection that can transport pockets of high-concentration fuel over long time scales. A volume of gas sinks along the cooler portion of the windows. Upon reaching the bottom, this flow turns and moves inward, displacing the fuel layer upward as a plume of high concentration of fuel, creating the local maxima consistently observed in all testing. Refraction produced by these pockets is too weak to be visualized with the BOS technique, but is observed in the IR absorption method and predicted by numerical simulation of natural convection within the cell.[1]

To investigate how the injected volume affects the dispersion of hexane in the cell, tests were conducted with four different liquid volumes: 50 µL, 75 µL, 100 µL, and 200 µL. Figure 8b shows the processed signals for the different injected volumes at 98.9°C. Measurements have been conducted in the middle of the cell. The time at which the concentration peak occurs increases with the fuel volume, rising from about 60 s at 50 μL to roughly 110 s at 200 μL. As a consequence, full mixing is achieved more rapidly for lower volumes. The four curves have very similar shapes, indicating that the qualitative behavior is independent of the injected volume.

The effect of the cell temperature on the dispersion of hexane was investigated at characteristic temperatures of hexane: lower than its boiling temperature (68.9°C), lower than its Leidenfrost temperature (∼99.9°C in our case), and higher than its AIT in our cell (∼231.9°C). The concentration measurements are shown in Fig. 9(a). The legend of the graph provides both the temperature at the center of the cell (T0) and the temperature of the lower plate (TS). The rate of dispersion increases with increasing temperature due to two temperature effects: 1) The diffusion constant is an increasing function of temperature; 2) For a fixed mass of liquid fuel, the thickness of the initial gaseous fuel increases with increasing temperature, as the density is inversely proportional to temperature at fixed pressure.

[1]The numerical simulations and comparisons with the experimental data will be reported in a subsequent publication that is under preparation.

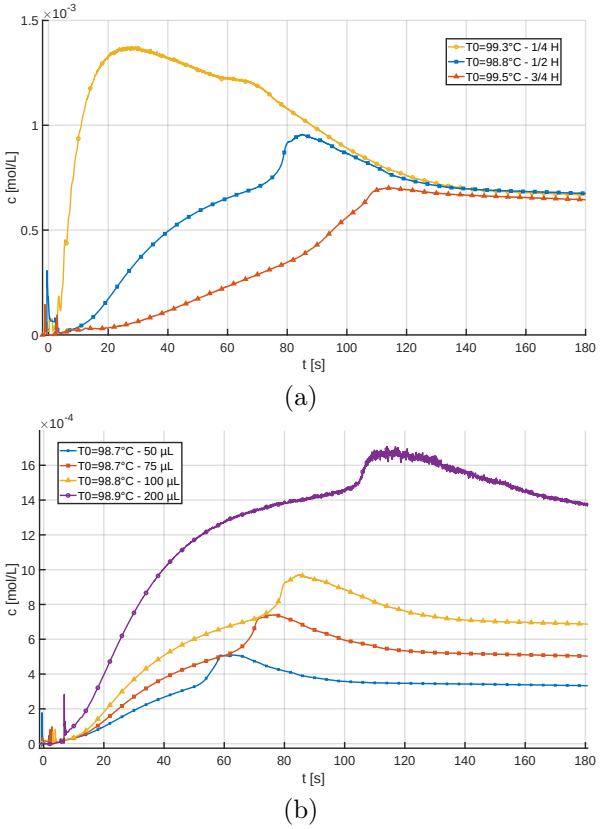


Figure 8: Effect of measurement location and liquid fuel volume on average fuel concentration. (a) Effect of measurement location, 100 µL of hexane. (b) Effect of liquid fuel volume, $H/2 = 5$ cm. The height of the cell H = 10 cm, the cell temperature T0 ∼ 99°C.

The concentration measurements show the transient competition between vapor expansion and diffusion. Immediately after injection, liquid hexane evaporates rapidly, causing a local increase in vapor concentration at the bottom of the cell. As time progresses, diffusion and convection disperse the fuel vapor throughout the cell. The transient peak observed in the concentration profile, identified as the result of natural convection mixing the fuel, has a magnitude that decreases as the temperature is reduced. Numerical simulations conducted in parallel with the experiments agree with this observation.

At and above the hexane autoignition temperature, chemical reactions rapidly consume hexane, resulting in a sharp decrease in fuel concentration. No ignition was observed for the 242.7°C test. A bright flame accompanied by a strong temperature

increase was observed for the 247.6°C test. A sharp increase in concentration was observed during the first seconds of the latest test. This increase is due to a vapor jet emitted from the needle before it was removed from the cell. When the needle becomes excessively hot, the fuel inside vaporizes abruptly, generating a jet that contributes to the mixing of the vapor.

To investigate the effect of convection on the dispersion and mixing of fuel, the bottom plate was set 20°C hotter than the top plate, resulting in natural convection inside the cell. The tests have been conducted with 100 µL at T0 = 106.9°C. The results comparing a case with and without natural convection at very similar T0 conditions are shown in Fig. 9b. It is visible that the convection speeds up the dispersion, resulting in a faster dispersion time. The peaks have almost identical heights, showing that the fuel concentrations along the laser path at the specific time are very similar. Thus, convection increases the dispersion speed and enhances the mixing of hexane with the air inside compared to mixing that relies solely on diffusion.

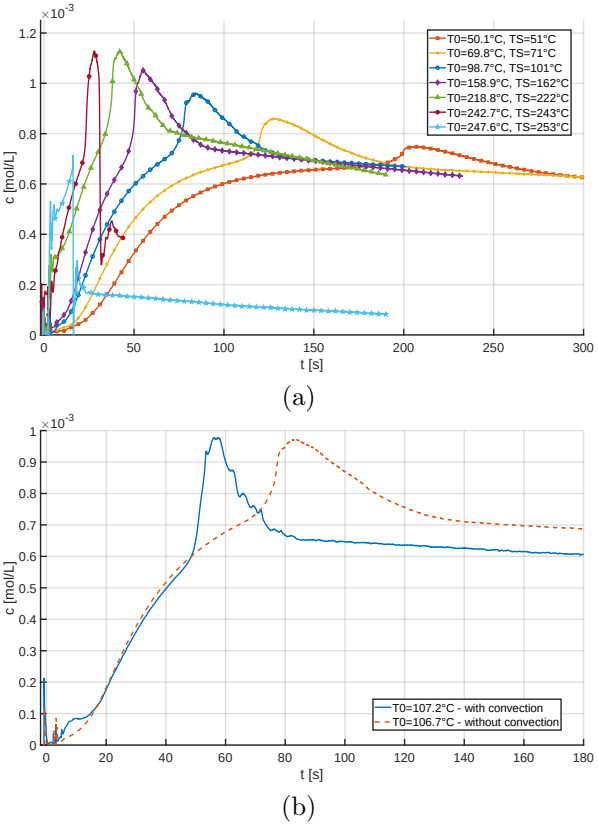


Figure 9: Effect of (a) cell temperature and (b) natural convection on the measured fuel concentration at the middle of the cell using 100 µL of hexane

3.3. Ignition observations

At temperatures below 220°C, obvious ignition events were not observed in our tests. This is consistent with the n-hexane AIT of 236°C used in hazard analysis (NFPA, 1991) and our previous measurements (Martin and Shepherd, 2021). Slow oxidation of the hexane does occur at lower temperatures over long durations (> 10 min) in vessels (Mével et al., 2019) and flow reactors (Mével et al., 2014). These low-temperature reactions in hydrocarbons do not result in significant temperature and pressure rise or visible light emission (Griffiths and Scott, 1987) but at temperatures comparable to the AIT temperatures, "cool flames" (Ju, 2021) appear, either in isolation at sub-atmospheric pressures or as part of the two-stage ignition process (Fish, 1968) at higher pressures. Cool flames have low energy release in comparison to high-temperature or "hot flames" with maximum temperatures on the order of 600°C and corresponding modest pressure increases. The slow rate of reaction within cool flames results in very slow flames, with measured speeds (Sueyasu and Hikita, 1965) of a few cm·s^{-1}, ten times smaller than typical hot flame speeds.

Cool flames and low-temperature oxidation reaction products are incompletely oxidized and can serve as fuel for a second stage of combustion, a rapidly propagating hot flame that results in substantial pressure rise, although less than that of a hot flame alone, and visible emission (Mével et al., 2019). In the range of temperatures just above the AIT (Fish, 1968), ignition proceeds in two stages, with the cool flame followed by a hot flame with temperatures up to 1700°C and nearly complete oxidation of any residual fuel and cool flame products. Two-stage ignition has been most intensively studied in the context of internal combustion engines (Bittle et al., 2011) at high pressure (10-30 atm), but comparable events are observed at atmospheric and subatmospheric pressures (Affleck, 1967). The process of two-stage ignition and formation of cool flames in n-hexane/air mixtures under autoignition conditions for $T < 630$°C is predicted by Davis et al. (2026). The total ignition delay time τ_{total} can be decomposed into a long period of formation τ_1 of precursor products before the appearance of a cool flame followed by hot ignition after a short

delay of duration τ_2, Fig. 10.

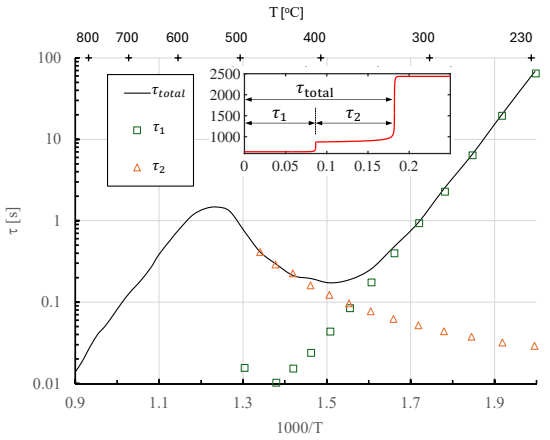


Figure 10: Predicted ignition delay times (Davis et al., 2026) for stoichiometric n-hexane/air mixtures at 1 atm. τ_{total} - time from inception to hot flame, τ_1 - time from inception to cool flame, τ_2 - time from cool to hot flame. Inset: example of constant pressure temperature-time history for ∼370°C.

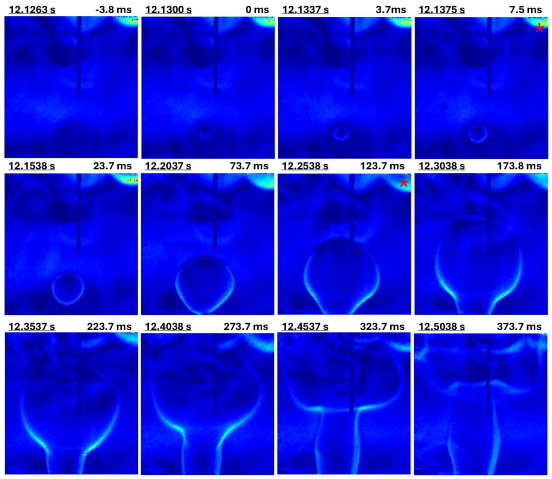
Although cool flames are predicted (Davis et al., 2026) to occur in AIT testing and categorized as a possible outcome ASTM-E659 (2014), to date the lack of optical access has precluded clear identification of cool flames and the existence of two-stage ignition processes. Martin and Shepherd (2021) categorized four distinct modes of ignition in their tests, although the relationship to cool flames and two-stage ignition could not be made. One of the goals of the present study was to make the connection between the empirical categories of Martin and Shepherd and the combustion science of cool flames and two-stage ignition. In the following subsections, measurements from selected tests are reported for both Mode I and Mode III events, documenting the presence of cool flames and two-stage ignition.

3.3.1. Two-stage ignition

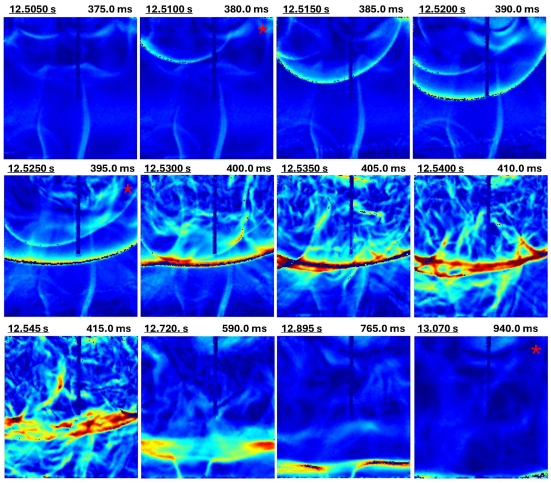
Figures 11a and 11b show the BOS-processed images of the two-stage ignition of 200 µL of hexane at 246.9°C. The colormap represents the displacement of the background as estimated by cross-correlation, with blue indicating low displacement and red corresponding to 4 px/frame. In this test, Mode I ignition was observed, as defined by Martin and Shepherd (2021), as a bright flame accompanied by a strong temperature increase in an ASTM test. The flame front is unstable, and the combustion results in large induced velocities, resulting in the appearance of significant fluctuations in the density gradients in the later stages of flame propagation.

The first stage occurs at 12.1300 seconds, where a small spherical region appears near the bottom of the cell. This region expands over time and propagates upward. Comparison with additional diagnostics (discussed later) indicates that this strong density gradient corresponds to the boundary of a cool flame, as defined by Davis et al. (2026). The visible emission of the cool flame is very faint and usually barely or not visible to the naked eye. The second stage occurs at 12.5050 seconds near the top of the cell, where a stronger density gradient forms and propagates downward more rapidly. This gradient delimits the extent of the hot flame, which is typically visible as a bright yellow or white emission. The hot flame stops propagating downward at 12.5250 seconds, when it encounters a region with an excessively high concentration of hexane vapor. As discussed in the previous section, the hexane vapor requires approximately 100-150 seconds to fully mix within the cell. At the time of ignition, the mixing process is still incomplete, and the hexane vapor is more concentrated near the bottom of the cell than at the top. All Mode I ignition cases studied in the cell exhibited the same two-stage ignition behavior.

The temperature measured during the same test by the thermocouple located at the center of the cell is shown in Fig. 12. Five key moments are marked on the graph, and the corresponding BOS images are indicated with an asterisk in Figs. 11a and b. These key moments are the formation of the cool flame kernel, the moment the cool flame reaches the thermocouple bead, the beginning of hot-flame propagation, the moment the hot flame reaches the thermocouple bead, and the time when the fuel is nearly completely consumed. The temperature begins to rise when the cool flame reaches the thermocouple bead, and no significant change is observed when the hot flame passes the bead. The temperature continues to increase even after the hot flame has finished propagating and the fuel is almost completely consumed. This behavior highlights the thermocouple's slow response time. The thermocouple leads are 34-gauge wire, 127 µm diameter. The bead formed by welding the wires to create the thermocouple junction is approximately 500 µm. Despite these small dimensions, the response time is too slow (time constant on the order of 50 to 100 ms) to accurately capture the rapid temperature variations across flame fronts.



(a)



(b)

Figure 11: Visualization of the first (a) and second (b) stage of Mode I ignition using BOS.

Figures 13a and 13b show the intensified sCMOS images of the two-stage ignition of 300 µL of hexane at 231.9°C. In this test, Mode I ignition was observed, as defined in Martin and Shepherd (2021) (*i.e.*, a bright flame accompanied by a strong temperature peak). The images present chemiluminescence at a wavelength around 313 nm, typical of excited hydroxyl radical (OH^*) spontaneous emission. The light intensity of each image has been independently adjusted to enhance visibility. The images show behaviors similar to those observed with the BOS technique, highlighting a two-stage process. Ignition occurs later than in the previous

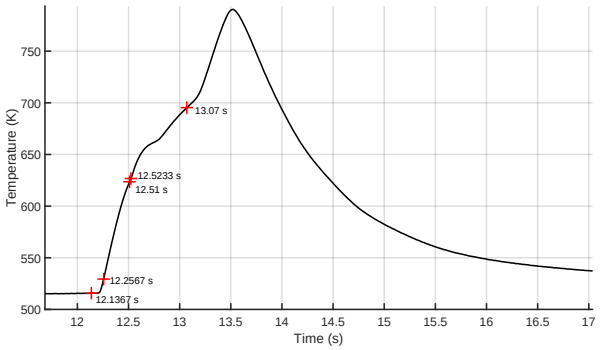
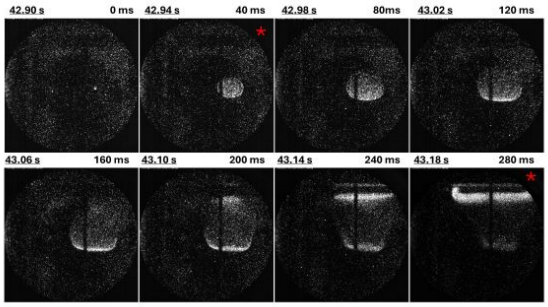


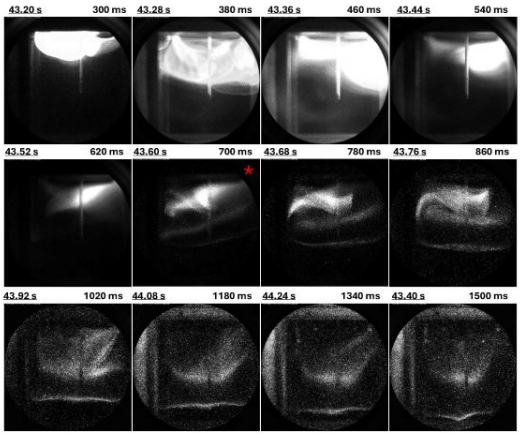
Figure 12: Temperature measurement for the events documented in Fig. 11.

test because the ignition delay time is temperature-dependent and the present test was performed at a lower temperature. The first stage (cool flame) combustion front visualized by OH^* chemiluminescence confirms that the low-density pocket of gas observed prior to hot-flame ignition in the BOS images is indeed created by a cool flame. The emission is weaker than that of the hot flame and requires binning to be detectable. A weak blue emission, visible to the naked eye in a completely dark laboratory, likely corresponds to excited C_2 or CH spontaneous emission. During the second stage, ignition occurs at the top of the cell, and a hot bright white/yellow flame propagates downward through the cell. Propagation ceases upon encountering a region where the hexane concentration is too rich to support combustion. The remaining hexane in the cell is then slowly consumed, accompanied by an orange flame.

Figure 14 shows the images acquired with the high-speed camera on the opposite side of the cell. The light intensity of each frame has been independently adjusted to improve visibility. The brightness of the cool flame is too low to be detected by the high-speed camera; only the bright white/orange hot flame is visible. This flame remains at the top of the cell, where the mixture is less fuel-rich due to a small leak around the vents that allows a slight amount of fresh air to enter. The remaining fuel burning slowly at the bottom of the cell is not visible to the high-speed camera. It should be noted that some artifacts appear in the images about two-thirds of the height on the left side. These result from reflections of the flame on the filter mounted on the intensified sCMOS camera positioned in front of the high-speed camera on



(a) First stage of Mode I ignition



(b) Second stage of Mode I ignition

Figure 13: Visualization of the first (a) and second (b) stage of Mode I ignition using intensified sCMOS images of OH* emission.

the opposite side of the cell.

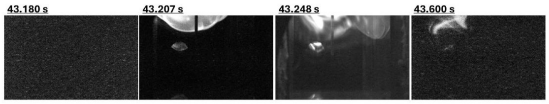
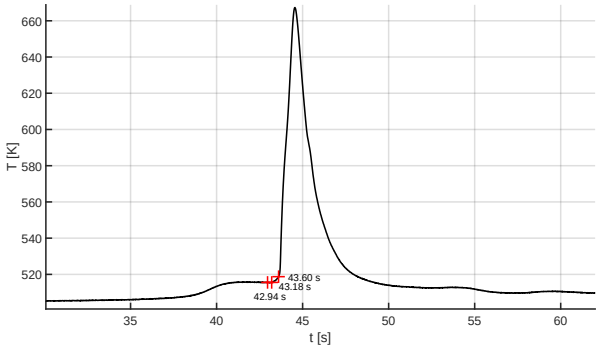
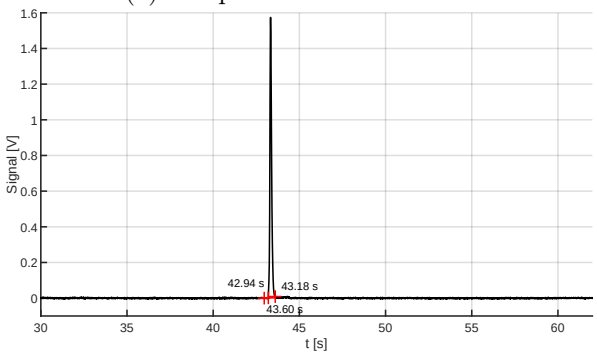


Figure 14: Selected high-speed digital video frames corresponding to the ignition events of Fig. 13.

The temperature measured during the same test by the thermocouple located at the center of the cell is shown in Fig. 15a. Three key moments are marked on the graph, and the corresponding intensified sCMOS images are indicated with an asterisk in Fig. 13: 42.92 s, the formation of the cool flame kernel; 43.18 s, the moment the cool flame reaches its lowest position (*i.e.*, where it ceases to propagate in the overly rich atmosphere); and 43.60 s, the moment the thermocouple begins to register a temperature increase. Compared to the 200 µL case, the height at which the atmosphere becomes too rich is above the thermocouple bead. As a result, the cool flame does not reach the thermocouple and therefore does not produce an increase in the measured temperature. The temperature rise is delayed until the hot flame has consumed enough fuel to progress downward and reach the thermocouple. It was also observed that the thermocouple begins to record a temperature increase at around 40 seconds, before the cool flame appears.



(a) Temperature measurement



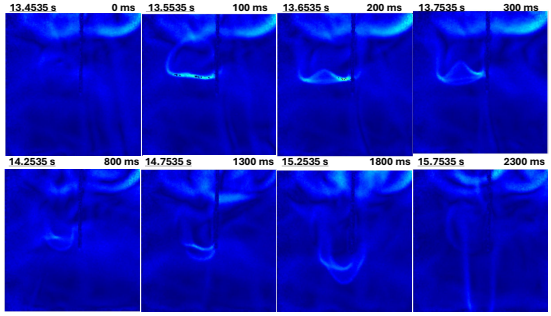
(b) Photodetector signal

Figure 15: Temperature (a) and photodetector (b) measurements for the ignition event associated with the intensified sCMOS measurements of Fig. 13.

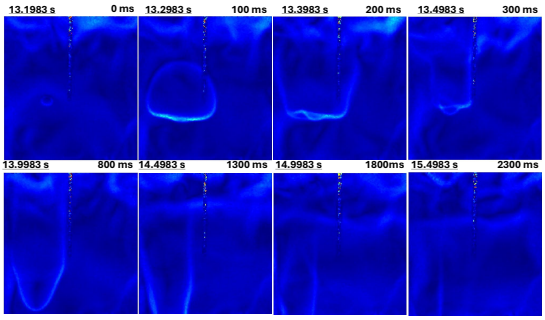
The signal measured during the same test by the photodetector is shown in Fig. 15b. As with the thermocouple signal, the same three key moments are marked on the graph. Consistent with the observations from the high-speed camera images, the cool flame is not detected by the photodetector because its emission is too weak and primarily in the UV range. In contrast, the hot flame emits a bright light that is clearly captured by the detector.

3.3.2. Cool flame propagation

Mode III ignition, defined by Martin and Shepherd (2021) as a large temperature increase without a bright flame, has also been observed in our tests. Figure 16a shows the BOS-processed images of Mode III ignition of 100 µL of hexane at 245.9°C. A cool flame kernel appears and propagates inside the cell. The temperature measured by the thermocouple in the middle of the cell increases when the cool flame touches it. The results indicate that Mode III ignition closely resembles the first ignition stage of Mode I and corresponds to the propagation of a cool flame through the gaseous mixture.



(a) Mode III ignition case



(b) No-ignition case

Figure 16: Visualization of cool flame propagation for Mode III and no-ignition using BOS. 100 µL of hexane at 246°C.

The cool flame can be localized and, in some cases, may not reach the thermocouple during its propagation. As a result, when a phenomenon similar to the previously shown Mode III ignition event occurs, no temperature rise is detected, and the operator records the test as a no-ignition event. Figure 17 shows the temperature trace from the Mode III case discussed above and compares it with a no-ignition case obtained under the same conditions (100 µL at 245.9°C). The BOS images for the no-ignition case are presented in Fig. 16b. Unlike the Mode III ignition case, the cool-flame propagation remains localized and does not spread throughout the cell. The kernel forms near the thermocouple but may lie slightly in front of or behind it, such that the cool flame does not make contact.

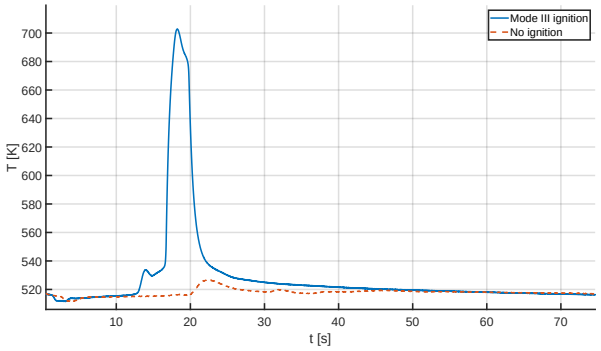


Figure 17: Temperature measurements associated with the Mode III ignition of Fig. 16a and the no-ignition cases of Fig. 16b.

4. Summary and Conclusions

Injection of liquid fuel droplets into a thermally stable atmosphere results in the formation of a dense fuel layer that subsequently mixes primarily by diffusion, a process that can take hundreds of seconds to form a uniform mixture, comparable to or longer than the time to ignition except for temperatures very close to the AIT. On the other hand, injection of fuel droplets into an unstable atmosphere or injection of the fuel as a gaseous jet can result in more rapid mixing of the fuel with the air.

The process of vaporization due to liquid impact on a hot surface occurs relatively rapidly compared to diffusion, but the droplet impact behavior and subsequent vaporization are strongly dependent on the temperature of the heated bottom surface and on the fuel properties. When the surface temperature is below the fuel boiling point, heat transfer is enhanced, and vaporization occurs rapidly. In contrast, when the surface temperature exceeds the fuel Leidenfrost temperature, the formation of a vapor layer between the liquid and the surface significantly reduces heat transfer and increases the evaporation time. This means that for short ignition delay times, fuels with Leidenfrost temperatures less than the AIT may be incompletely vaporized before ignition takes place.

Once the fuel has vaporized, a layer of concentrated fuel forms at the bottom of the cell, temporarily suppressing the convection cells that may have developed due to minor temperature gradients prior to injection. This layer gradually mixes into the surrounding atmosphere, with diffusion driving the process in the absence of convection. The time required for preexisting convection cells to reestablish depends on the temperature gradients along the cell vertical walls. Convection cells develop more rapidly when the temperature gradients are larger, and the injected fuel volume is smaller. Once these convection cells have formed, they induce more mixing of the fuel, eventually resulting in a fully homogenized atmosphere.

Low-temperature chemistry results in cool flames preceding hot flames, so rather than these being distinct ignition modes, they represent a two-stage ignition process. These two stages were successfully visualized experimentally, confirming the numerical predictions of Davis et al. (2026). The first stage consists of long-duration, low-temperature combustion that is followed by a slowly moving cool flame emitting dim light primarily in the ultraviolet range. The flame kernel is created in the lower regions of the cell, where the fuel concentration is highest, and rises toward the top via convection. The second stage is the formation of a hot flame within the cool flame kernel, producing a rapidly propagating flame, identified by intense luminosity and elevated temperatures. At temperatures near, but below, the autoignition temperature (AIT) of hexane, a cool flame may develop without progressing to a hot flame. This cool flame can generate a thermocouple response similar to that of a hot flame due to the thermocouple's limited response time when exposed to the steep temperature gradients of a hot flame. If the flame is sufficiently localized, it may go undetected, as it does not come into direct contact with the sensor bead.

5. Implications for the standardized autoignition testing

The thermal environment and fuel injection methods for our tests are very similar to what is used in many standardized autoignition tests. Based on the present results and our previous studies (Davis et al., 2025, 2026), it is concluded that in standardized testing, ignition may occur before the fuel has sufficient time to fully mix with the surrounding atmosphere. As a consequence, the fuel oxidation processes take place in a temporally evolving, spatially nonuniform mixture. The composition cannot be characterized based on an average value computed from the mass of fuel injected and mass of air in the test vessel. Although the present study was conducted with a single fuel, we anticipate that many of the present findings regarding vaporization and mixing apply to a wide range of liquid hydrocarbon fuels. Testing is in progress to generalize the results to larger molecules and commodity fuels, particularly regarding ignition behavior.

A great deal of emphasis is placed in standardized testing on achieving a highly uniform temperature within the test vessel (Davis et al. (2025)). However, having an extremely thermally stable atmosphere and injecting liquid fuels as droplets will lengthen the mixing time compared to having a slightly unstable atmosphere and/or injecting the fuel as a high-speed gas jet, which will dramatically increase the mixing rate. Vaporization of the liquid fuel within the test volume may also create significant local thermal fluctuations in the region of the vaporizing fuel. Enhancing the mixing through mechanical means (jets or stirring) and injection of gaseous fuels rather than liquid drops will create more uniform initial temperature and concentration conditions in standardized testing.

For hexane, the autoignition temperature (AIT) exceeds its Leidenfrost temperature, resulting in a vaporization behavior during autoignition tests that differs markedly from that of fuels such as some jet fuels, whose Leidenfrost temperatures are higher than their respective AITs. Mizomoto and Ikai (1978) demonstrated the relationship between ignition time and surface temperature while investigating the ignition of a cetane droplet on a hot plate, highlighting distinct behaviors below and above the Leidenfrost temperature that may influence the outcome of autoignition testing.

In previous work (Fouchier and Shepherd, 2025), the authors reported different ignition modes while investigating aviation fuels. Mode I and Mode III, as defined by Martin and Shepherd (2021), correspond respectively to (i) a bright-flame ignition accompanied by a strong temperature rise and (ii) no visible flame or only a very weak blue flame accompanied by a large temperature rise. In that study, these two modes exhibited similar temperature signatures during ignition and were distinguished solely by the presence or absence of a bright orange/white flame. In the present work, clear

differences between Mode I and Mode III are observed for hexane. Mode I ignition features a two-stage process involving a cool flame followed by a hot, bright flame. When the hexane concentration is near the stoichiometric value, Mode I can produce a substantial pressure increase that triggers the opening of the vents. Mode III ignition, by contrast, involves only the propagation of the cool flame and does not generate a significant pressure rise. The two-step ignition process observed is consistent with the numerical simulations by Davis et al. (2026) for ASTM testing with n-hexane. It is anticipated based on past research (Fish, 1968; Griffiths and Scott, 1987) that two-stage ignition events also occur in AIT testing for other hydrocarbon fuels and fuel blends, but further study is needed to generalize from n-hexane to commodity fuels.

The thermocouple signals for the two ignition modes are so similar that an operator could not reliably distinguish between them based on the signals alone. This behavior is attributed to the thermocouple response time. Even though a gauge-34 thermocouple is used, the hot flame evolves too rapidly for the sensor to capture its temperature accurately, whereas the cool flame propagates more slowly. As a result, both flames produce similar thermocouple responses, despite the large difference in their actual temperatures. Near the autoignition limit, events recorded as "no ignition" may still involve a cool flame, but one that is sufficiently localized that it does not affect thermocouple measurements.

These findings indicate that it is not possible to discriminate between hot and cool flame ignitions (Mode I and Mode III events) in the ASTM E659 test with thermocouple data alone. The ASTM E659 standard requires the reported AIT to be based on the lowest temperature observed for hot flame ignition over the range of fuel concentration tested. The authors suggest that any efforts to improve the standard by using additional instrumentation to automate testing and remove operator bias should focus on the detection of luminosity using photodetectors and analysis of signal amplitude rather than thermocouple signals to discriminate between cool and hot flames. However, as discussed in Fouchier and Shepherd (2025), faster digital recording of the thermocouple signal coupled with synchronization to automated injection will obtain data that can be exceedingly useful in improving the methodology of experimentation. With sufficiently precise ignition delay times as a function of temperature, it is possible to create Arrhenius plots, logarithm of ignition delay *vs.* reciprocal temperature, that can be used to dramatically speed up the process of identifying the limiting temperature for hot flame ignition in conjunction with the luminosity measurements.

Acknowledgements

This research was carried out in the Explosion Dynamics Laboratory of the California Institute of Technology. Financial support was from the Boeing Company through a Strategic Research and Development Relationship Agreement (CT-BA-GTA-1) and Dr. Fouchier was supported by the HORIZON-MSCA-2021 Postdoctoral Fellowship Program, Project # 101063624. The authors thank Ash Parbala of Scientific Imaging, Inc for arranging the loan of the intensified sCMOS camera. Noel Esparza-Duran and Jason Kamau assisted with fabrication and preliminary testing.

References

Affleck, W.S., 1967. Two-stage ignition under engine conditions parallels that at low pressures, in: 11th Symposium (International) on Combustion, Elsevier. pp. 1003–1013.

ASTM-E659, 2014. Standard test method for autoignition temperature of liquid chemicals. American Society for Testing and Materials.

Bittle, J.A., Knight, B.M., Jacobs, T.J., 2011. Two-Stage Ignition as an Indicator of Low-Temperature Diesel Combustion. Combustion Science and Technology 183, 947–966.

Chen, C.C., Hsieh, Y.C., 2010. Effect of experimental conditions on measuring autoignition temperatures of liquid chemicals. Industrial & engineering chemistry research 49, 5925–5932.

Davis, B., Fouchier, C., Shepherd, J.E., 2025. Fluid motion and heat transfer in an ASTM-E659 apparatus. Journal of Loss Prevention in the Process Industries 94, 105558.

Davis, B., Shepherd, J.E., Mével, R., 2026. Numerical modeling of gaseous n-hexane autoignition in an ASTM-E659 apparatus. Fuel 405, 136691.

Fish, A., 1968. The Cool Flames of Hydrocarbons. Angewandte Chemie International Edition in English 7, 45–60.

Fouchier, C., Shepherd, J.E., 2025. ASTM-E659 standardized test analysis and results for synthetic paraffinic kerosene. Journal of Loss Prevention in the Process Industries 94, 105568.

Goodwin, D.G., Moffat, H.K., Schoegl, I., Speth, R.L., Weber, B.W., 2023. Cantera: An object-oriented software toolkit for chemical kinetics, thermodynamics, and transport processes. https://www.cantera.org. doi:10.5281/zenodo.8137090. version 3.0.

Griffiths, J., Scott, S., 1987. Thermokinetic interactions: Fundamentals of spontaneous ignition and cool flames. Progress in Energy and Combustion Science 13, 161–197.

Ju, Y., 2021. Understanding cool flames and warm flames. Proceedings of the Combustion Institute 38, 83–119.

Kirar, P.K., Kumar, N., Sahu, K.C., 2024. Dynamics of jet breakup and the resultant drop size distribution-effect of nozzle size and impingement velocity. Physics of Fluids 36, 102108.

Liang, G., Mudawar, I., 2017. Review of drop impact on heated walls. International Journal of Heat and Mass Transfer 106, 103–126.

Martin, C.D., 2023. Experiments in Thermal Ignition: Influence of Natural Convection on Properties of Gaseous Explosions. Ph.D. thesis. California Institute of Technology.

Martin, C.D., Shepherd, J.E., 2021. Low temperature autoignition of Jet A and surrogate jet fuel. Journal of Loss Prevention in the Process Industries 71, 104454.

Mével, R., Boettcher, P.A., Shepherd, J.E., 2012. Absorption cross section at 3.39 μm of alkanes, aromatics and substituted hydrocarbons. Chemical Physics Letters 531, 22–27.

Mével, R., Chatelain, K., Boettcher, P., Dayma, G., Shepherd, J., 2014. Low temperature oxidation of n-hexane in a flow reactor. Fuel 126, 282–293.

Mével, R., Rostand, F., Lemarié, D., Breyton, L., Shepherd, J., 2019. Oxidation of n-hexane in the vicinity of the auto-ignition temperature. Fuel 236, 373–381.

Mills, A.A., Fry, J.D., 1982a. Rate of evaporation of hydrocarbons from a hot surface: Nukiyama and leidenfrost temperatures. European Journal of Physics 3, 152–154.

Mills, A.A., Fry, J.D., 1982b. Rate of evaporation of hydrocarbons from a hot surface: Nukiyama and Leidenfrost temperatures. European Journal of Physics 3, 152–154.

Mizomoto, M., Hayano, H., Ikai, S., 1978. Evaporation and Ignition of a Fuel Droplet on a Hot Surface (Part 1, Evaporation). Bulletin of the JSME-Japan Society of Mechanical Engineers 21, 1765–1771.

Mizomoto, M., Ikai, S., 1978. Evaporation and Ignition of a Fuel Droplet on a Hot Surface (Part 2, Ignition). Bulletin of the JSME-Japan Society of Mechanical Engineers 21, 1772–1779.

Mizomoto, M., Morita, A., Ikai, S., 1979. Evaporation and Ignition of a Fuel Droplet on a Hot Surface (Part 3, Effects of Initial Droplet Diameter). Bulletin of the JSME-Japan Society of Mechanical Engineers 22, 1266–1273.

NFPA, 1991. Fire protection guide to hazardous materials. 10th ed., National Fire Protection Association.

Raffel, M., 2015. Background-oriented schlieren (BOS) techniques. Experiments in Fluids 56, 60.

Setchkin, N.P., 1954. Self-ignition temperatures of combustible liquids. Journal of Research of the National Bureau of Standards 53, 49.

Stamhuis, E., Thielicke, W., 2014. PIVlab–towards user-friendly, affordable and accurate digital particle image velocimetry in MATLAB. Journal of open research software 2, 30.

Sueyasu, S., Hikita, T., 1965. Study of low temperature flames of n-hexane. Combustion and Flame 9, 1–6.

Werner, R., Mayhew, E., Kim, K., Kweon, C.B., Michael, J.B., 2024. Examining surface wetting and Leidenfrost transition of jet fuels and bicomponent mixtures. Experimental Thermal and Fluid Science 154, 111167.